ARTICLES

Journal of Semiconductors
(2020) 41, 062301
doi: 10.1088/1674-4926/41/6/062301

Modelling and optical response of a compressive-strained AlGaN/GaN quantum well laser diode

A. Menani[1], L. Dehimi[1, 2], S. Dehimi[3], and F. Pezzimenti[4, †]

[1]Laboratory of Metallic and Semiconducting Materials (LMSM), Department of Electrical Engineering, Biskra University, Biskra, Algeria

[2]Faculty of Science, Elhadj Lakhdar University, Batnal, Algeria

[3]Research Centre in Industrial Technology (CRTI), Algiers, Algeria

[4]DIIES – Mediterranea University of Reggio Calabria, Reggio Calabria, Italy

Abstract: The effects of the quantum well (QW) width, carrier density, and aluminium (Al) concentration in the barrier layers on the optical characteristics of a gallium nitride (GaN)-based QW laser diode are investigated by means of a careful modelling analysis in a wide range of temperatures. The device's optical gain is calculated by using two different band energy models. The first is based on the simple band-to-band model that accounts for carrier transitions between the first levels of the conduction band and valence band, whereas the second assumes the perturbation theory (k.p model) for considering the valence intersubband transitions and the relative absorption losses in the QW. The results reveal that the optical gain increases with increasing the n-type doping density as well as the Al molar fraction of the $Al_xGa_{1-x}N$ layers, which originate the GaN compressive-strained QW. In particular, a significant optical gain on the order of 5000 cm^{-1} is calculated for a QW width of 40 Å at room temperature. In addition, the laser threshold current density is of few tens of A/cm^2 at low temperatures.

Key words: laser diode; quantum well; optical gain; threshold current; temperature

Citation: A Menani, L Dehimi, S Dehimi, and F Pezzimenti, Modelling and optical response of a compressive-strained AlGaN/GaN quantum well laser diode[J]. *J. Semicond.*, 2020, 41(6), 062301. http://doi.org/10.1088/1674-4926/41/6/062301

1. Introduction

In the last few decades, gallium arsenide (GaAs) alloys and III–V semiconductors were the most commercialized materials for laser diodes (LDs)[1, 2]. However, although GaAs technology is mature and GaAs-based lasers are well known for their high efficiency in converting electricity into monochromatic light, the emission of coherent light is limited in the red and infrared regions of the optical spectrum[3–7]. Therefore, due to the small bandgap of these materials, III–V semiconductors are unsuitable for the fabrication of short-wavelength optical devices[8–15].

An important challenge in the field of optoelectronics is the development of short wavelength lasers which can emit coherent light in green, blue, violet, and ultraviolet (UV) regimes. In particular, III-nitride and IV wide bandgap materials have received a great attention for the promising realization of several devices[16–24]. These devices are able to operate at high power levels and high temperatures, due to their mechanical hardness and larger band offset[25–32]. Recently, GaN-based high efficiency short wavelength light emitting diodes (LEDs) and LDs have been commercialized by achieving apparent improvements in terms of crystal quality and conductivity control in solid-state lighting and high-density optical storage systems. In addition, one of the most interesting features of GaN is the realization of the wurtzite-type crystal for semiconductor lasers. Although zinc-blend GaN has also been studied, it still does not have as good qualities as the wurtzite crystal[33, 34].

In this paper, the optical gain and threshold current density of a compressive-strained AlGaN/GaN quantum well (QW) laser, which emits in the UV regime, have been investigated in a wide range of temperatures by means of the Atlas-Silvaco physical device simulator. The optical gain spectra have been calculated by using a simple parabolic band model and also a multiband formalism based on the perturbation theory (k.p model) that is particularly suited for crystals with wurtzite symmetry. In the first case, we have assumed the electron and hole wavefunctions calculated by taking into account transitions that occur only between the first levels of the conduction band and valence band (band-to-band model) similarly to Ref. [35]. In the second case, we have considered the intervalence band absorption effects from different energy levels, namely heavy-hole (HH), light-hole (LH), and split-off (SO), computed via a 6 × 6 k.p model in the QW region[36, 37]. This model, accounting for an intermixing of states in the valence subbands, provides a much more accurate coupling with the conduction band for an improved laser diode optical response. The calculated optical gain is around 5000 cm^{-1} for a QW width of 40 Å and an Al molar fraction of 0.1 at room temperature. The dependence of the laser threshold current density from temperature has been also investigated.

2. Calculation models and parameters

The optical gain can be defined as the fractional increase in photons per unit of length in response to a given photon flux[33]. The optical gain expression as a function of

Correspondence to: F Pezzimenti, fortunato.pezzimenti@unirc.it
Received 19 SEPTEMBER 2019; Revised 5 DECEMBER 2019.
©2020 Chinese Institute of Electronics

the photon energy $h\omega$ is in the form[38]

$$G_{\rm opt}(h\omega)=\frac{\pi e^2}{n_{\rm r}c\omega m_0^2\varepsilon_0}\sum_{n,m}\int\frac{m_{\rm r}}{\pi h^2 L_{\rm w}}\frac{\Gamma/(2\pi)}{(E-h\omega)^2+(\Gamma/2)^2}\times\left(f_{\rm c}^n-f_{\rm v}^m\right)|I_{m,n}|^2|M_{\rm b}|^2{\rm d}E, \tag{1}$$

where ε_0 is the free-space dielectric constant, $n_{\rm r}$ is the material refractive index, h is Planck's constant, c is the light velocity, e is the electron charge, E is the transition energy, $I_{m,n}$ is the overlap integral of electron and hole wavefunctions, Γ is the line-width due to Lorentzian broadening, $L_{\rm w}$ is the well width, $M_{\rm b}$ is the polarization-dependent bulk momentum matrix element, m_0 is the carrier mass in free-space, and $m_{\rm r}=(m_{\rm c}^{-1}+m_{\rm v}^{-1})^{-1}$ is the reduced effective mass which depends on the valence ($m_{\rm v}$) and conduction ($m_{\rm c}$) band effective masses. Finally, in Eq. (1), the sum is taken all over the transitions between the electron and hole subband energy levels, labelled in the following as E_n and E_m, and the Fermi-Dirac distribution functions $f^n{}_{\rm c}$ and $f^m{}_{\rm v}$ are described by using

$$f_{\rm c}^n(E)=\frac{1}{1+\exp\left\{\left[E_n+(m_{\rm r}/m_{\rm c})(E-E_{mn})-E_{F_{\rm c}}\right]/kT\right\}}, \tag{2}$$

$$f_{\rm v}^m(E)=\frac{1}{1+\exp\left\{\left[E_m-(m_{\rm r}/m_{\rm v})(E-E_{mn})-E_{F_{\rm v}}\right]/kT\right\}}, \tag{3}$$

where $E_{mn}=E_n-E_m$, and $E_{F_{\rm c}}$ and $E_{F_{\rm v}}$ are the electron and hole quasi-Fermi levels, respectively. To calculate the optical gain, therefore, we have to calculate the QW subband energies and the relative electron and hole wavefunctions in the device active region, namely the GaN layer situated between the two AlGaN barrier layers. The strain effect and the strong built-in field effect due to the piezoelectric polarization of III-nitride materials have been carefully taken into account in the calculations of the laser optical gain.

A schematic diagram of the energy band structure assumed for modelling and simulations is shown in Fig. 1.

By using the perturbation theory in considering the valence intersubband transitions, the hole energy states have been computed via a 6 × 6 diagonalized k.p Hamiltonian matrix in the form of[36, 37]:

$$H_{6\times6}^v(K)=\begin{bmatrix}H_{3\times3}^U(K) & 0\\ 0 & H_{3\times3}^L(K)\end{bmatrix}, \tag{4}$$

where $H_{3\times3}^U(K)$ and $H_{3\times3}^L(K)$ are 3 × 3 matrices given by

$$H^U(K)=\begin{bmatrix}F & K_t & -iH_t\\ K_t & G & \Delta-iH_t\\ iH_t & \Delta+iH_t & \lambda\end{bmatrix}, \tag{5}$$

$$H^L(K)=\begin{bmatrix}F & K_t & iH_t\\ K_t & G & \Delta+iH_t\\ -iH_t & \Delta-iH_t & \lambda\end{bmatrix}. \tag{6}$$

These matrix elements, which contain the general expressions for a strained semiconductor, can be expressed as follows:

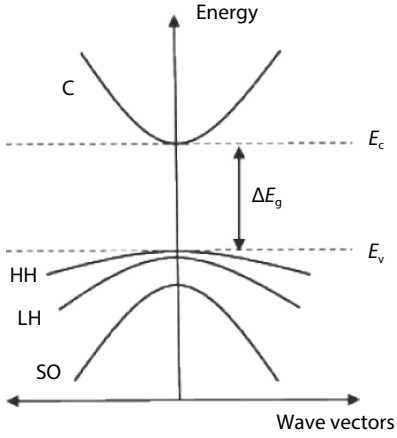

Fig. 1. Schematic diagram showing the energy band states in the QW: conduction (C), heavy-hole (HH), light-hole (LH), and split-off (SO).

$$F=\Delta_1+\Delta_2+\lambda+\theta, \tag{7}$$

$$G=\Delta_1-\Delta_2+\lambda+\theta, \tag{8}$$

$$\lambda=\frac{\hbar^2}{2m_0}\left(A_1k_z^2+A_2k_t^2\right)+D_1\varepsilon_{zz}+D_2\left(\varepsilon_{zz}+\varepsilon_{yy}\right), \tag{9}$$

$$\theta=\frac{\hbar^2}{2m_0}\left(A_3k_z^2+A_4k_t^2\right)+D_3\varepsilon_{zz}+D_4\left(\varepsilon_{zz}+\varepsilon_{yy}\right), \tag{10}$$

$$K_t=\frac{\hbar^2}{2m_0}A_5k_z^2, \tag{11}$$

$$H_t=\frac{\hbar^2}{2m_0}A_6k_tk_z, \tag{12}$$

$$\Delta=\sqrt{2}\Delta_3, \tag{13}$$

where A_{1-6} are hole effective mass parameters, Δ_{1-3} are split energies, D_{1-4} are shear deformation potentials, k_t and k_z are wave vectors along the device x–y basal plane and z-direction, respectively. In addition, the strain tensors relative to the lattice constant mismatch between the QW and barrier layers, i.e. ε_{xx}, ε_{yy}, and ε_{zz}, are modelled through the expressions:

$$\varepsilon_{xx}=\varepsilon_{yy}=\frac{a_1-a_0}{a_0}, \tag{14}$$

$$\varepsilon_{zz}=\frac{c_1-c_0}{c_0}, \tag{15}$$

where a_i and c_i are lattice constants in the device structure.

The polarization modelling includes both the spontaneous polarization ($P_{\rm sp}$), which is strain independent, and the piezoelectric polarization along the growth direction <0001> given by[39, 40]:

$$P_{\rm pz}=2d_{\rm pz}\left(C_{11}+C_{12}-2\frac{C_{13}^2}{C_{33}}\right)\varepsilon_{xx}, \tag{16}$$

where the terms C_{ij} are elastic constants and $d_{\rm pz}$ is an oppor-

Table 1. Material parameters for wurtzite nitride binaries at $T = 300$ K.

Parameter	GaN	AlN
E_g (eV)	3.4	6.25
α (meV/K)	0.90	1.799
β (K)	830	1462
m_c/m_0	0.20	0.33
m_v/m_0	0.8	0.25
a	3.189	3.112
c	5.185	4.982
Δ_1 (eV)	0.01	−0.169
$\Delta_2 = \Delta_3$ (eV)	0.0056	0.0063
A_1	−7.21	−3.86
A_2	−0.44	−0.25
A_3	6.68	3.58
A_4	−3.46	−1.32
A_5	−3.40	−1.47
A_6	−4.90	−1.64
D_1 (eV)	−3.7	−11.8
D_2 (eV)	4.50	7.90
D_3 (eV)	8.20	8.80
D_4 (eV)	−4.1	−3.90
C_{11} (GPa)	390	396
C_{12} (GPa)	145	137
C_{13} (GPa)	106	108
C_{33} (GPa)	398	373
d_{pz} (pm/V)	−1.6	−2.1
P_{sp} (C/m^2)	−0.034	−0.09

tune coefficient.

The reference parameters of the binary compounds GaN and AlN (wurtzite crystals) are summarized in Table 1[41]. Here, α and β are the coefficients that describe the nonlinear temperature dependence of the bandgap energy E_g according to the expression[42]

$$E_g(T) = E_g - \frac{\alpha T^2}{\beta + T}. \tag{17}$$

In addition, for a specific $Al_xGa_{1-x}N$ ternary alloy, the variation of E_g due to the effective Al molar fraction x was calculated by using[42, 43]

$$E_g(x, T) = xE_g^{AlN}(T) + (1-x)E_g^{GaN}(T) - 0.6x(1-x), \tag{18}$$

where the so-called bowing parameter fixed to 0.6 accounts for the deviation from a linear interpolation between the values of $E_g^{AlN}(T)$ and $E_g^{GaN}(T)$ calculated by considering that the coefficients α and β are also dependent on x as follows:

$$\alpha(x) = (1-x)\alpha_{GaN} + x\alpha_{AlN} - 2.15x(1-x), \tag{19}$$

$$\beta(x) = (1-x)\beta_{GaN} + x\beta_{AlN} - 1561x(1-x). \tag{20}$$

Finally, Adachi's refractive index model aids to calculate the $Al_xGa_{1-x}N$ x-dependent refractive index as[38]

$$n_r(\omega) = \sqrt{A\left(\frac{\hbar\omega}{E_g}\right)^{-2}\left(2 - \sqrt{1+\frac{\hbar\omega}{E_g}} - \sqrt{1-\frac{\hbar\omega}{E_g}}\right) + B}, \tag{21}$$

where the material parameters A and B are in the form

$$A(x) = 9.827 - 8.216x - 31.59x^2, \tag{22}$$

$$B(x) = 2.736 + 0.842x - 6.293x^2. \tag{23}$$

For a single QW with a width L_w, the threshold current density can be written as[44]

$$J_{th} = qL_w n_{th}/\tau_{th}, \tag{24}$$

where n_{th} and τ_{th} are the threshold carrier density and lifetime, respectively. By increasing the temperature, the intrinsic losses of the laser diode tend to increase while the device internal efficiency factor tends to decrease. The variation of the threshold current with temperature is assumed in the form[45]:

$$J_{th}(T) = J_{th}\exp\frac{T - T_0}{T_0}, \tag{25}$$

where J_{th} is the reference value at a given temperature, and T_0 is a specific parameter that determines the effective degradation of the diode conduction capabilities and therefore the resulting increase of the laser threshold current. This temperature parameter was calculated for AlGaN-based laser diodes by fitting experimental data on J_{th} in Ref. [14]. In particular, T_0 was estimated to be 132 K in the low temperature range and it drops down to 89 K for T higher than about 395 K.

3. Results and discussion

The investigated device structure consists of a GaN active layer situated between two 80-nm-thick $Al_xGa_{1-x}N$ barrier regions. By fixing $x = 0.1$ and $L_w = 40$ Å as entry data for simulations, the optical gain spectrum is firstly calculated as a function of the wavelength for different carrier densities in the range 1×10^{18}–1×10^{19} cm^{-3} as shown in Fig. 2. The value $n = 1 \times 10^{18}$ cm^{-3} can, in fact, be assumed as the threshold carrier density (transparency density) for the considered device. As we can see, the increase of the injection level in the active region determines the increase of the maximum optical gain for both the band-to-band and 6-band k.p models. These behaviours are due to the filling of high states in the conduction band and valence band with the resulting increase of the emission phenomena as reported for similar laser structures[46, 47]. In addition, the observable shift of the emission spectrum towards the shorter wavelengths is explained on the basis of the quantization effects that tend to increase the transition energy of the bound states and therefore the emission wavelength decreases following the standard expression $\lambda = hc/E$[48].

The curves in Figs. 2(a) and 2(b) are, however, quite different each other. In fact, the optical gain values in Fig. 2(b) are strongly increased if compared to those reported in Fig. 2(a) as a consequence of the intermixing of available states in the valence subbands. In addition, the gain spectrum calculated using the band-to-band model is rather wide as a consequence of the large energy difference between the quasi-Fermi levels which results from the model assumptions.

The optical gain dependence on the Al molar fraction for $n = 1 \times 10^{19}$ cm^{-3} is shown in Fig. 3.

It is worth noting that in $Al_xGa_{1-x}N$/GaN QW lasers an increasing value of x meaningfully increases the maximum op-

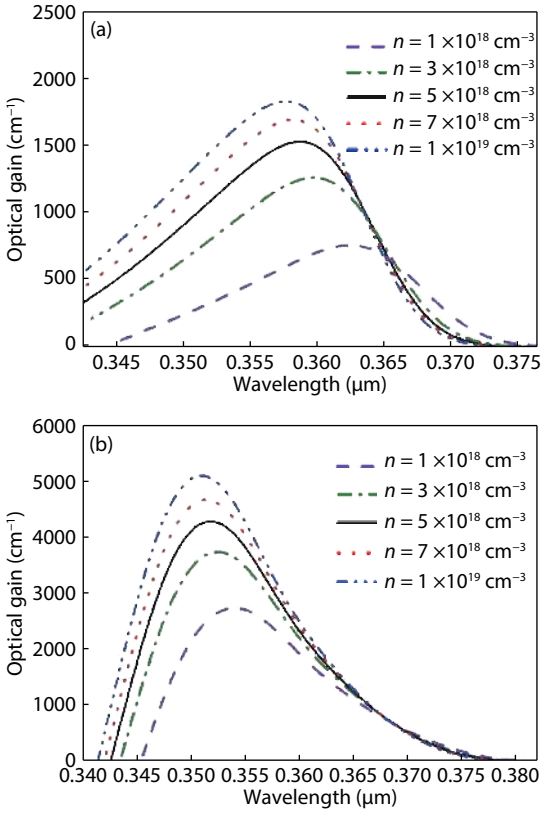

Fig. 2. (Color online) Optical gain spectrum in an $Al_{0.1}Ga_{0.9}N/GaN/Al_{0.1}Ga_{0.9}N$ QW laser as a function of the wavelength for different carrier densities in the active region at $T = 300$ K. (a) Band-to-band model. (b) 6-band k.p model.

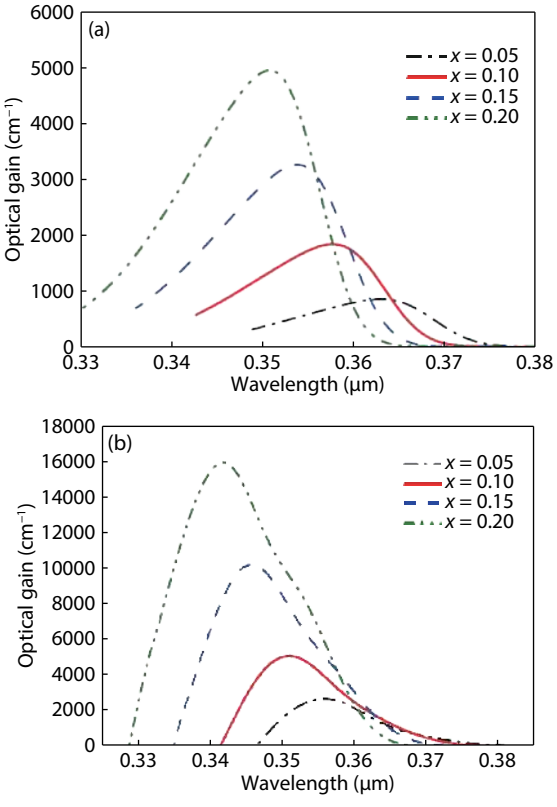

Fig. 3. (Color online) Optical gain spectrum as a function of the Al molar fraction at $T = 300$ K. (a) Band-to-band model. (b) 6-band k.p model.

tical gain moving the gain spectrum towards the shorter wavelengths. This shift is due to the increase of the $Al_xGa_{1-x}N$ bandgap, calculated as wide as 3.896 eV for $x = 0.2$, and the change of the quantization energy. At the same time, the increase of the maximum gain value is mainly due to the increase in the optical confinement because the refractive index of the barrier layers tends to become higher than that in the GaN active region.

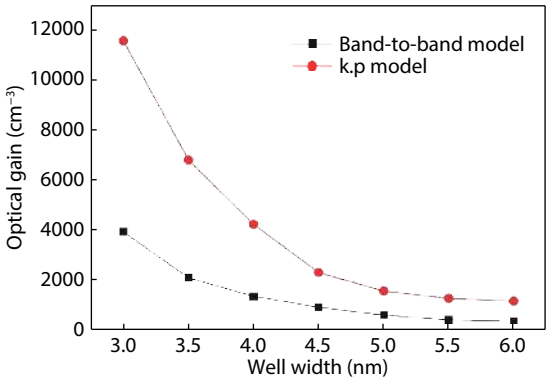

Fig. 4. (Color online) Optical gain spectrum as a function of the GaN QW width ($x = 0.1$ and $n = 1 \times 10^{19}$ cm^{-3}) at $T = 300$ K.

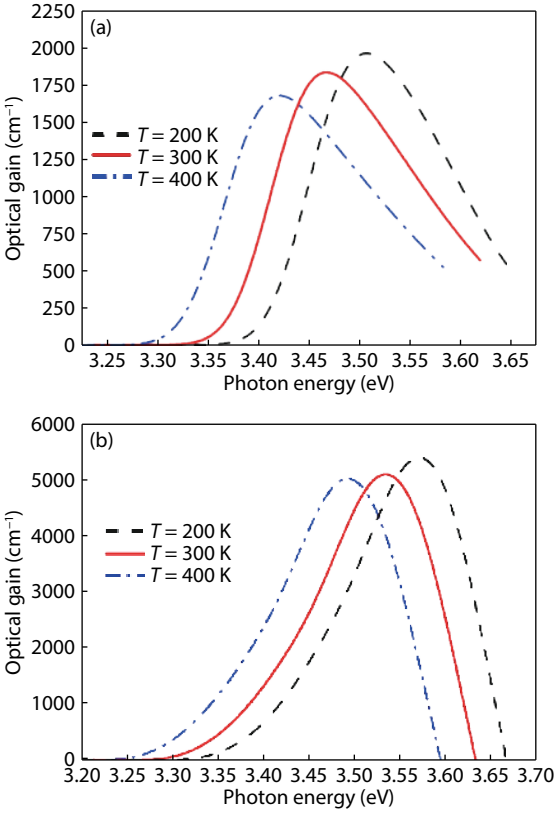

Fig. 5. (Color online) Dependence of the optical gain on temperature ($L_w = 40$ Å, $x = 0.1$, and $n = 1 \times 10^{19}$ cm^{-3}). (a) Band-to-band model. (b) 6-band k.p model.

A fundamental geometrical parameter in the design of the considered device is the width of the GaN well (L_w). The plot of the maximum optical gain calculated for different values of L_w in the range 30 to 60 Å is shown in Fig. 4. A wider QW penalizes increasingly the optical gain and L_w = 40 Å should be assumed as a limit value in this study. The wider the QW, the stronger electrons and holes are separated by the piezoelectric field and therefore the optical gain reduces. In other words, when the QW width increases, the density of states in this region decreases.

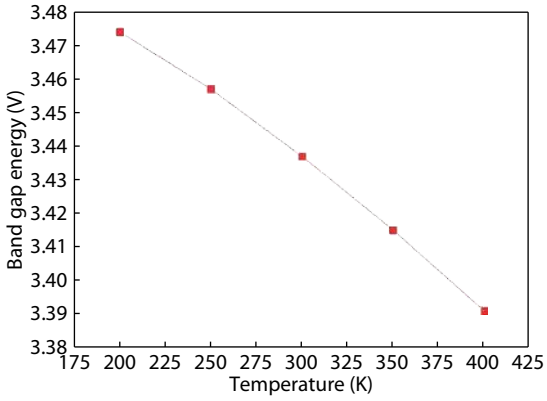

Fig. 6. (Color online) GaN bandgap energy as a function of the temperature.

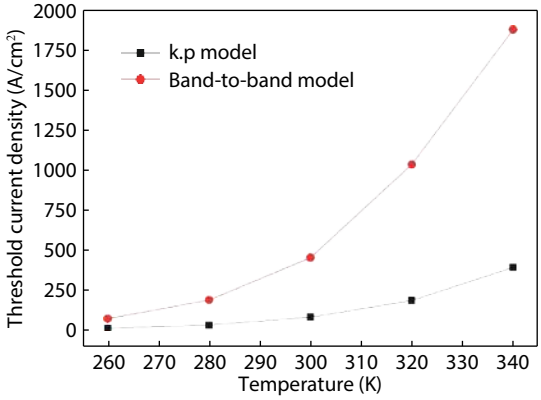

Fig. 7. (Color online) Threshold current density dependence on temperature ($L_w = 40$ Å, $x = 0.1$, and $n = 1 \times 10^{19}$ cm^{-3}).

The temperature effects on the optical gain behaviour are shown in Fig. 5. Here, it is evident that the temperature has only a limited impact on the maximum gain value. In more detail, the optical gain tends to decrease as the temperature increase in accordance with the variation of the Fermi-Dirac distributions in Eqs. (2) and (3). Meanwhile, by increasing the temperature, the GaN bandgap shrinks and carriers can scatter to other subbands leading to a change of the spectrum range that tends to shift toward the lower photon energies.

The temperature-dependent GaN bandgap profile is shown in Fig. 6. The interatomic spacing increases when the amplitude of the atomic vibrations increases due to an increased thermal energy. This effect causes a dilatation of the lattice and leads to a displacement of the conduction and valence band edges.

Finally, the laser threshold current density variation with temperature in the range 260–340 K is shown in Fig. 7.

By using the k.p model, the increase of the threshold current density with temperature is stronger than the simple band-to-band behaviour. This increase is on the order of a factor 5 at T = 340 K. The minimum J_{th} value is around 60 A/cm^2 for both models at very low temperatures.

4. Conclusion

In this paper, we have investigated the optical response of a strained wurtzite GaN/$Al_xGa_{1-x}N$ quantum well laser. The effects of the carrier density, quantum well width, Al concentration in the barrier layers, and temperature have been taken into account by using two different band energy models in the device structure. In particular, the optical gain increases by increasing the carrier density as well as the Al concentration whereas it decreases with the quantum well width and temperature. The simulation analysis based on the k.p model, with a more accurate calculation, provides better results in terms of optical gain reducing also the dependence of the threshold current density on temperature. Our analysis suggests that laser diodes based on a GaN/AlGaN QW can emit in the UV with a significant optical gain and a low threshold current density.

References

[1] Nakamura S, Fasol G. The blue laser diode. Berlin: Springer, 1997
[2] Zory P S. Quantum well lasers. New York: Academic Press, 1993
[3] Kieleck C, Eichhorn M, Hirth A, et al. High-efficiency 20–50 kHz mid-infrared orientation-patterned GaAs optical parametric oscillator pumped by a 2 μm holmium laser. Opt Lett, 2009, 34, 262
[4] Liu H C, Dudek R, Shen A, et al. High absorption quantum-well infrared photodetectors. Appl Phys Lett, 2001, 79, 4237
[5] Bouzid F, Pezzimenti F, Dehimi L, et al. Analytical modeling of dual-junction tandem solar cells based on an InGaP/GaAs heterojunction stacked on a Ge substrate. J Electron Mater, 2019, 48, 4107
[6] Ustinov V M, Zhukov A E. GaAs-based long-wavelength lasers. Semicond Sci Technol, 2000, 15, R41
[7] Rogalski A. Infrared detectors: an overview. Infrared Phys Tech, 2002, 43, 187
[8] Justice J, Bower C, Meitl M, et al. Wafer-scale integration of group III–V lasers on silicon using transfer printing of epitaxial layers. Nat Photonics, 2012, 6, 610
[9] Bouzid F, Dehimi L, Pezzimenti F, et al. Numerical simulation study of a high efficient AlGaN-based ultraviolet photodetector. Superlattice Microstruct, 2018, 122, 57
[10] Dehimi S, Dehimi L, Aissat A. Study and Simulation of a quantum well structure based ZnTe/Zn_xCd_{1-x}Te/ZnTe. Proc International Conference of Renewable Energy – CIER, 2014
[11] Liu H, Wang T, Jiang Q, et al. Long-wavelength InAs/GaAs quantum-dot laser diode monolithically grown on Ge substrate. Nat Photonics, 2011, 5, 416
[12] Della Corte F G, De Martino G, Pezzimenti F, et al. Numerical simulation study of a low breakdown voltage 4H-SiC MOSFET for photovoltaic module-level applications. IEEE Trans Electron Devices, 2018, 65, 3352
[13] De Martino G, Pezzimenti F, Della Corte F G, et al. Design and numerical characterization of a low voltage power MOSFET in 4H-SiC for photovoltaic applications. Proc IEEE International Conference Ph. D. Research in Microelectronics and Electronics – PRIME, 2017
[14] Yoshida H, Kuwabara M, Yamashita Y, et al. AlGaN-based laser diodes for the short-wavelength ultraviolet region. New J Phys, 2009, 11, 125013
[15] Bouzid F, Dehimi L, Pezzimenti F. Performance analysis of a Pt/n-GaN Schottky barrier UV detector. J Electron Mater, 2017, 46, 6563
[16] DenBaars S P, Feezell D, Kelchner K, et al. Development of gallium-nitride-based light-emitting diodes (LEDs) and laser diodes for energy-efficient lighting and displays. Acta Mater, 2013, 61, 945
[17] Marouf Y, Dehimi L, Pezzimenti F. Simulation study for the current matching optimization in $In_{0.48}Ga_{0.52}N/In_{0.74}Ga_{0.26}N$ dual junction solar cells. Superlattice Microstruct, 2019, 130, 377
[18] Bencherif H, Dehimi L, Pezzimenti F, et al. Improving the efficiency of a-Si: H/c-Si thin heterojunction solar cells by using both

antireflection coating engineering and diffraction grating. Optik, 2019, 182, 682

[19] Zeghdar K, Dehimi L, F Pezzimenti F, et al. Simulation and analysis of the current-voltage-temperature characteristics of Al/Ti/4H-SiC Schottky barrier diodes. Jpn J Appl Phys, 2019, 58, 014002

[20] Fritah A, Dehimi L, Pezzimenti F, et al. Analysis of *I–V–T* characteristics of Au/n-InP Schottky barrier diodes with modeling of nanometer-sized patches at low temperature. J Electron Mater, 2019, 48, 3692

[21] Farrell R M, Haeger D A, Hsu P S, et al. High-power blue-violet AlGaN-cladding-free m-plane InGaN/GaN laser diodes. Appl Phys Lett, 2011, 99, 171113

[22] Bouzid F, Pezzimenti F, Dehimi L, et al. Numerical simulations of the electrical transport characteristics of a Pt/n-GaN Schottky diode. Jpn J Appl Phys, 2017, 56, 094301

[23] Bencherif H, L Dehimi L, Pezzimenti F, et al. Analytical model for the light trapping effect on ZnO: Al/c-Si/SiGe/c-Si solar cells with an optimized design. Proc International Conference on Applied Smart Systems – ICASS, 2018

[24] Marouf Y, Dehimi L, Bouzid F, et al. Theoretical design and performance of $In_xGa_{1-x}N$ single junction solar cell. Optik, 2018, 163, 22

[25] Monroy E, Guillot F, Leconte S, et al. III-nitride nanostructures for infrared optoelectronics. Acta Phys Pol A, 2006, 110, 295

[26] Rao S, Pangallo G, Pezzimenti F, et al. High-performance temperature sensor based on 4H-SiC Schottky diodes. IEEE Electron Device Lett, 2015, 36, 720

[27] De Martino G, Pezzimenti F, Della Corte F G. Interface trap effects in the design of a 4H-SiC MOSFET for low voltage applications. Proc International Semiconductor Conference – CAS, 2018

[28] Bencherif H, Dehimi L, Pezzimenti F, et al. Temperature and SiO_2/4H-SiC interface trap effects on the electrical characteristics of low breakdown voltage MOSFETs. Appl Phys A, 2019, 125, 294

[29] Megherbi M L, Pezzimenti F, Dehimi L, et al. Analysis of different forward current-voltage behaviours of Al implanted 4H-SiC vertical p–i–n diodes. Solid-State Electron, 2015, 109, 12

[30] Bencherif H, Dehimi L, Pezzimenti F, et al. Multiobjective optimization of design of 4H-SiC power MOSFETs for specific applications. J Electron Mater, 2019, 48, 3871

[31] Ikeda M, Mizuno T, Takeya M, et al. High-power GaN-based semiconductor lasers. Phys Status Solidi, 2004, 6, 1461

[32] Pezzimenti F, Bencherif H, Yousfi A, et al. Current–voltage analytical model and multiobjective optimization of design of a short channel gate-all-around-junctionless MOSFET. Solid-State Electron, 2019, 161, 107642

[33] Asgari A, Dashti S. Optimization of optical gain in $Al_xGa_{1-x}N$/GaN/Al_xGa_{1-x} N strained quantum well laser. Optik, 2012, 123, 1546

[34] Schubert E F, Kim J K. Solid-state light sources getting smart. Science, 2005, 308, 1274

[35] Ohtoshi T, Yamaguchi K, Nagaoka C, et al. A two dimensional device simulator of semiconductor lasers. Solid-State Electron, 1987, 30, 627

[36] Chuang S L, Chang C S. k.p method for strained wurtzite semiconductors. Phys Rev B, 1996, 54, 2491

[37] Chuang S L. Optical gain of strained wurtzite GaN quantum-well lasers. IEEE J Quantum Electron, 1996, 32, 1791

[38] Silvaco TCAD. Atlas user's manual device simulation software. California: Silvaco Int., 2016

[39] Bernardini F, Fiorentini V. Spontaneous versus piezoelectric polarization in III –V Nitrides: Conceptual aspects and practical consequences. Phys Status Solidi B, 1999, 216, 391

[40] Ambacher O, Majewski J, Miskys C, et al. Pyroelectric properties of Al(In)GaN/GaN heteroand quantum well structures. J Phys Condens Mat, 2002, 14, 3399

[41] Vurgaftman I, Meyer J R. Nitride semiconductor devices. New York: Wiley, 2007

[42] Nepal N, Li J, Nakarmi M L, et al. Temperature and compositional dependence of AlGaN the energy band gap of alloys. Appl Phys Lett, 2005, 87, 242104

[43] Dakhlaoui H. Linear and nonlinear optical absorption coefficients and refractive index changes in GaN/$Al_xGa_{1-x}N$ double quantum wells operating at 1.55 μm. J Appl Phys, 2015, 117, 1357051

[44] Dehimi S, Dehimi L, Asar T, et al. Modelling of a Cd_{1-x} Zn_xTe/ZnTe single quantum well for laser diodes. J Electron Mater, 2017, 46, 775

[45] Casey H C, Panish M B. Heterostructure lasers. New York: Academic Press, 1978

[46] Dehimi S, Dehimi L, Asar T, et al. Modeling and simulation of $Zn_xCd_{1-x}Te$/ZnTe quantum well structure for laser applications. Optik, 2017, 135, 153

[47] Dehimi S, Aissat A, Haddad D, et al. Optimization of optical gain in $In_xGa_{1-x}Sb$/GaSb unstrained quantum well structures. Enrgy Proced, 2015, 74, 191

[48] Aissat A, Nacer S, Ykhlef F, et al. Modeling of $Ga_{1-x}In_xAs_{1-y-z}N_y$-$Sb_z$/GaAs quantum well properties for near-infrared lasers. Mater Sci Semicond Proc, 2013, 16, 1936